Cell, Vol. 93, 125–138, April 3, 1998, Copyright ©1998 by Cell Press

# Crystal Structure of the Thermosome, the Archaeal Chaperonin and Homolog of CCT

**Lars Ditzel,* Jan Löwe,*§ Daniela Stock,*§ Karl-Otto Stetter,† Harald Huber,† Robert Huber,* and Stefan Steinbacher*‡**

*Max-Planck-Institut für Biochemie
Am Klopferspitz 18a
D-82152 Martinsried
Germany

†Institut für Mikrobiologie
Universität Regensburg
Universitätsstrasse 31
D-93053 Regensburg
Germany

## Summary

**We have determined to 2.6 Å resolution the crystal structure of the thermosome, the archaeal group II chaperonin from *T. acidophilum*. The hexadecameric homolog of the eukaryotic chaperonin CCT/TRiC shows an $(\alpha\beta)_4(\alpha\beta)_4$ subunit assembly. Domain folds are homologous to GroEL but form a novel type of inter-ring contact. The domain arrangement resembles the GroEL-GroES *cis*-ring. Parts of the apical domains form a lid creating a closed conformation. The lid substitutes for a GroES-like cochaperonin that is absent in the CCT/TRiC system. The central cavity has a polar surface implicated in protein folding. Binding of the transition state analog Mg-ADP-$AlF_3$ suggests that the closed conformation corresponds to the ATP form.**

## Introduction

Chaperonins are essential multisubunit assemblies that promote facilitated protein folding in concert with ATP hydrolysis (reviewed by Ellis and Hartl, 1996; Hartl, 1996). They have been identified in all three taxonomic domains and are divided into two distinct classes based on their evolutionary lineage (reviewed by Willison and Kubota, 1994). Group I chaperonins occur in eubacteria (GroEL: Georgopoulos et al., 1973) and in the endosymbiotically derived mitochondria (Hsp60: Cheng et al., 1989) and chloroplasts (Rubisco-subunit-binding protein: Hemmingsen et al., 1988) of eukaryotic cells. Group II chaperonins are found in archaea (thermosomes: Phipps et al., 1991; TF55: Trent et al., 1991) and the evolutionarily related cytosol of eukaryotes (CCT: Frydman et al., 1992; Gao et al., 1992; Yaffe et al., 1992).

Our current understanding of the action of chaperonins originates from extensive work on GroEL as the prototype of group I chaperonins (reviewed by Fenton and Horwich, 1997). In the absence of nucleotide or in the presence of Mg-ADP, chaperonins provide an interactive surface with high affinity for nonnative or partially folded proteins prone to aggregation (Staniforth et al., 1994). This interaction seems to be largely independent of the structure or sequence of the substrate proteins (Viitanen et al., 1992; Horwich et al., 1993), but exposed hydrophobic regions appear to be a common feature for substrate recognition (Fenton et al., 1994). Bound substrate molecules are released in an ATP-dependent manner from the binding regions and are encapsulated in a closed compartment where folding proceeds (Weissman et al., 1995; Hayer-Hartl et al., 1996; Mayhew et al., 1996). Several rounds of binding and release may be required to reach the folded state (Weissman et al., 1994; Mayhew et al., 1996; Rye et al., 1997). A characteristic of group I chaperonins is that they depend on cochaperonins 10 for the release of folded polypeptides (GroES: Tilly et al., 1981; Langer et al., 1992). Binding of GroES to GroEL supports a conformational rearrangement switching GroEL from a high-affinity state for substrate-polypeptides to a low-affinity state (Weissman et al., 1995). In addition, GroES modulates the cooperativity of the intrinsic GroEL ATPase (Gray and Fersht, 1991; Yifrach and Horovitz, 1994).

The conformational states associated with the functional cycle of GroEL have been characterized both by electron microscopy (Roseman et al., 1996) and X-ray crystallography (Braig et al., 1994; Xu et al., 1997a). The GroES heptamer forms a dome structure (Hunt et al., 1996; Mande et al., 1996) that closes the central channel of GroEL by binding to the apical domains upon nucleotide-dependent domain rearrangements (Chen et al., 1994). Electron microscopy has revealed both football-shaped, symmetric $GroES_7$:$GroEL_{14}$:$GroES_7$ complexes (Azem et al., 1994; Llorca et al., 1994 ; Schmidt et al., 1994) and bullet-shaped, asymmetric $GroEL_{14}$:$GroES_7$ complexes (Langer et al., 1992; Saibil et al., 1993; Chen et al., 1994; Engel et al., 1995). The latter have been identified as the folding-active state of GroEL (Hayer-Hartl et al., 1995; Mayhew et al., 1996; Weissman et al., 1996). The crystal structure of the asymmetric $GroEL_{14}$:$GroES_7$:$(ADP)_7$ complex (Xu et al., 1997a) demonstrates how elevation and twist of the apical domains, stabilized by GroES binding, doubles the volume of the *cis*-cavity and changes its character from hydrophobic to hydrophilic. The change from a hydrophobic to a hydrophilic character of the folding chamber is thought to be the key step in chaperonin-assisted protein folding.

Group II chaperonins in archaea and in the eukaryotic cytosol have been shown to use the same mechanism as group I chaperonins, comprising the binding of substrate to a central cavity (Marco et al., 1994a) and ATP-dependent substrate release (Frydman et al., 1992; Gao et al., 1992; Yaffe et al., 1992; Farr et al., 1997). Sequence comparison (Lewis et al., 1992; Kim et al., 1994) and electron microscopy studies (Phipps et al., 1993; Marco et al., 1994a) have indicated a structural relationship between the two chaperonin groups. This relationship is supported by a recent crystal structure of an isolated apical domain of a thermosome $\alpha$ subunit (Klumpp et al., 1997).

Group I chaperonins such as GroEL consist of two

‡To whom correspondence should be addressed.
§Present address: MRC Laboratory of Molecular Biology, Hills Road, Cambridge CB2 2QH, UK.

heptameric rings, whereas group II chaperonins consist of two stacked octameric (thermosomes: Phipps et al., 1993; Andrä et al., 1996; CCT: Marco et al., 1994a) or nonameric rings (TF55: Knapp et al., 1994; Marco et al., 1994b). Archaeal group II chaperonins are composed of one (Andrä et al., 1996) to two (Waldmann et al., 1995) different subunits, whereas eukaryotic group II chaperonins have eight different subunits (Kubota et al., 1994). This may reflect an evolution toward more specialized chaperonins with a common scaffolding in the equatorial domains but divergent polypetide-binding sites in the apical domains (Kim et al., 1994). Whereas a multitude of proteins interact with GroEL in vitro and in vivo (Ewalt et al., 1997), the group II chaperonin of the eukaryotic cytosol CCT has a restricted range of substrates. Its only established in vivo substrates are actin, tubulin (Frydman et al., 1992; Gao et al., 1992; Yaffe et al., 1992; Sternlicht et al., 1993), and Gα-transducin (Farr et al., 1997). However, more polypeptides can bind to CCT in vitro (Melki et al., 1997). The ability of group II chaperonins to function without cochaperonins 10 raises the question of whether their mechanism differs from that of group I chaperonins. Here we present the crystal structure of the thermosome from the archaeon *Thermoplasma acidophilum* in unliganded form and in complex with different nucleotides and nucleotide analogs.

## Results and Discussion

### Structure Determination

Thermosomes were purified from *T. acidophilum* with a yield of 8 mg from 10 g of cells, reflecting the high abundance in this organism. Crystallization under high-salt conditions both in the absence of nucleotide and magnesium and in the presence of Mg-ADP yielded three independent crystal forms (Table 1 and Experimental Procedures). The nucleotide-free crystals of space group I422 with one αβ-dimer in the asymmetric unit diffracted X-rays to 2.9 Å resolution on in-house sources and to 2.4 Å with synchrotron radiation but suffered from severe radiation damage. All cryo conditions tested resulted in complete loss of diffraction. The effective resolution of in-house data collected at room temperature was limited to about 3.1 Å. High-resolution synchrotron data collected at room temperature were merged from up to 30 crystals (Table 1). Multiple isomorphous replacement resulted in an electron density map at 4.0 Å resolution that could be readily interpreted guided by the atomic model of GroEL (Boisvert et al., 1996). The model of the thermosome includes residues α17–α519 and β20–β521; the N- and C-terminal residues α1–α16, β1–β19, α520–α545, and β522–β543 are disordered. The model of unliganded thermosome was refined to an R-factor of 21.5% and an R-free of 29.8% at 2.6 Å resolution (Table 1).

### General Architecture

The thermosome is composed of two stacked eight-membered rings of alternating α and β subunits. The lower and upper rings are related by 2-fold symmetry, generating α-α and β-β pairs, respectively. This results in an $(\alpha\beta)_4(\alpha\beta)_4$ arrangement with 42-point symmetry (Figure 1A). The overall shape of the complex is spherical rather than cylindrical, with a height of 158 Å along the pseudo 8-fold axis and a diameter of 164 Å along the 2-fold axes. The bullet-shaped GroEL-GroES complex is 184 Å high and measures 140 Å in diameter (Figure 1B). In the thermosome, a large central cavity is sequestered from the environment as the entrance along the pseudo 8-fold axis is blocked by a lid domain unique to group II chaperonins (Figure 1C).

### Subunit Structure

The fold and domain arrangement of the α and β subunits of the thermosome are virtually identical. The Cα atoms can be superimposed with an rmsd value of 1.1 Å within secondary structural elements. The overall sequence identity is 60% with only one 2-residue insertion at position β146 (Figure 2). Therefore, the structural description and residue numbering in this report will be confined to the α subunit. As would be expected by the 46% sequence similarity between GroEL and the thermosome, the subunits share a basic fold with an equatorial, intermediate, and apical domain (Braig et al., 1994) (Figure 3A). This has also been observed in the crystal structure of an isolated apical domain of the thermosome α subunit (Klumpp et al., 1997). Superposition of Cα atoms of individual thermosome domains with the domains from a subunit of the GroEL-GroES *cis*-ring (*trans*-ring, in parentheses) shows rmsd values of 1.4 (1.8) Å, 1.2 (1.4) Å, and 1.7 (1.4) Å for the equatorial, intermediate, and apical domains, respectively. The high degree of structural conservation demonstrates that the domains are inflexible structures, in agreement with the observed nature of GroEL domain movements as rigid body motions (Xu et al., 1997a). The pivot points that connect the domains, corresponding to Pro-137/Gly-410 and Gly-192/Gly-375 in GroEL, are present in group II chaperonins as well but differ in the length of the loop regions (Figure 2).

Whereas the equatorial and intermediate domains of the thermosome have only small insertions and deletions compared to GroEL, the apical domains show a large deletion of 35 residues comprising helices K and L in GroEL. An insertion forming a lid segment extends helix H in GroEL by 18 residues at the N-terminal end and is preceded by two β strands, S12 and S13, giving a total of 28 inserted residues (Figure 2).

The detailed domain arrangement of a thermosome subunit on the whole resembles that observed in the *cis*-ring of the GroEL-GroES complex (Figures 1A and 1B), where it is stabilized by nucleotide and GroES binding. In comparison to the *trans*-ring, the intermediate domains are tilted onto the equatorial domains, closing the nucleotide-binding sites. However, a superposition of the entire subunits of the GroEL *cis*-ring and the thermosome results in a large rmsd value of 4.1 Å for Cα atoms of conserved secondary structural elements (Figure 2). This is mainly due to a clockwise rotation of the apical domain of the thermosome by approximately 15° when looking along the 2-fold axis of the particle.

### Intra-Ring Contacts

Each α subunit has a surface area of 22,360 $Å^2$, 73% of which is hydrophilic. The intra-ring contacts with the β

Table 1. Data Collection and Phasing Statistics

| Statistics[a] | NATI | MAGS | MAFS | MADS | MADC1 | MADC2 | | |
|---|---|---|---|---|---|---|---|---|
| Limiting resolution (Å) | 2.6 | 3.1 | 3.2 | 3.2 | 2.9 | 2.8 | | |
| Unique reflections | 42,095 | 23,954 | 22,043 | 20,729 | 31,989 | 64,854 | | |
| Mean redundancy | 3.9 | 2.7 | 3.5 | 2.2 | 2.2 | 3.3 | | |
| Completeness (%) | 93.6 | 89.7 | 92.0 | 86.0 | 89.4 | 91.0 | | |
| $R_{sym}$ (%) | 6.6 | 11.0 | 11.3 | 12.2 | 9.1 | 8.3 | | |
| Unit cell dimensions | | | | | | | | |
| a, b (Å) | 168.3 | 168.7 | 167.8 | 168.7 | 195.8 | 155.8 | | |
| c (Å) | 203.4 | 203.7 | 202.3 | 203.9 | 167.8 | 246.0 | | |
| Spacegroup | I422 | I422 | I422 | I422 | I422 | I4 | | |
| Quality of Native Dataset | | | | | | | | |
| Resolution (Å) | 20.0–6.55 | 4.76 | 3.93 | 3.42 | 3.07 | 2.80 | 2.60 | Overall |
| Completeness (%) | 96.9 | 99.7 | 99.5 | 98.5 | 97.4 | 96.4 | 77.3 | 93.6 |
| $I/\sigma_I$ | 10.7 | 11.7 | 11.7 | 8.9 | 5.8 | 3.3 | 2.5 | 8.6 |
| $R_{sym}$ (%) | 4.5 | 5.3 | 5.4 | 7.5 | 12.4 | 22.1 | 28.9 | 6.6 |
| MIR Analysis[b] | | TABR1 | TABR2 | TACL | AUCN | PTCL | GDAT | |
| Limiting resolution (Å) | | 4.2 | 5.0 | 4.3 | 4.0 | 4.5 | 4.0 | |
| Unique reflections | | 10,685 | 6,359 | 10,020 | 12,132 | 7,850 | 11,838 | |
| Mean redundancy | | 3.2 | 3.3 | 3.4 | 4.3 | 3.0 | 2.6 | |
| Completeness (%) | | 96.2 | 96.9 | 97.6 | 92.4 | 88.6 | 94.1 | |
| $R_{sym}$ (%) | | 15.0 | 9.9 | 18.8 | 12.7 | 12.9 | 11.3 | |
| $R_{iso}$ (%) | | 20.3 | 29.5 | 25.8 | 24.1 | 18.6 | 23.5 | |
| Number of sites | | 4 | 4 | 3 | 3 | 3 | 3 | |
| Phasing power | | 1.42 | 2.74 | 1.35 | 0.9 | 0.79 | 0.64 | |
| $R_c$ | | 0.68 | 0.51 | 0.72 | 0.89 | 0.89 | 0.94 | |
| Mean figure of merit at 4.0 Å | 0.51 | | | | | | | |
| Refinement Statistics | NATI | MAGS | MAFS | MADS | MADC1 | MADC2 | | |
| Resolution range (Å) | 8.0–2.6 | 8.0–3.1 | 8.0–3.2 | 8.0–3.2 | 8.0–2.9 | 8.0–2.8 | | |
| Reflections | 39,576[c] | 22,638 | 20,792 | 19,488 | 30,303[c] | 62,741[c] | | |
| Non-hydrogen atoms | 7,582 | 7,642 | 7,648 | 7,638 | 7,603 | 15,276 | | |
| $R_{work}$ (%) | 21.5 | 19.1 | 18.1 | 18.3 | 20.9 | 23.8 | | |
| $R_{free}$ (%) | 29.8 | 28.5 | 28.5 | 29.2 | 27.8 | 29.8 | | |
| rms bond length (Å) | 0.011 | 0.011 | 0.012 | 0.011 | 0.011 | 0.012 | | |
| rms bond angle (°) | 1.6 | 1.7 | 1.6 | 1.7 | 1.7 | 1.6 | | |
| rms bonded B (Å$^2$) | 4.3 | 3.8 | 4.4 | 3.8 | 4.0 | 3.8 | | |
| rms NCS atoms (Å) | — | — | — | — | — | 0.14 | | |
| rms NCS B (Å$^2$) | — | — | — | — | — | 2.2 | | |

[a] NATI: native dataset. Nucleotide bound complexes were obtained by soaking of crystals in nucleotide containing crystallization buffer (MADS: 3 mM ADP, 7.5 mM $MgCl_2$, 48 hr; MAGS: 3 mM ATP$\gamma$S, 7.5 mM $MgCl_2$, 12 hr; MAFS: 2 mM ADP, 5 mM $MgCl_2$, 3 mM $KAl(SO_4)_2$, 20 mM KF, 18 hr) or by cocrystallization (the precipitant solution was supplemented with 3 mM ADP and 7.5 mM $MgCl_2$ [MADC1 and MADC2]).

[b] Heavy-atom derivatives were prepared by soaking of crystals in heavy-atom-containing crystallization buffer. TABR1: 0.5 mM $Ta_6Br_{14}$, 2 hr. TABR2: 5 mM $Ta_6Br_{14}$, 15 min; TACL: 0.5 mM $Ta_6Cl_{14}$, 18 hr. AUCN: 2 mM $KAu(CN)_2$, 13 hr. PTCL: 0.5 mM $K_2PtCl_2$, 16 hr. GDAT: 20 mM $GdCl_3$/10 mM ATP, 13 hr. In TABR1, TABR2, and TACL the clusters bound to the same sites but differed in their relative occupancies.

[c] Reflections with $|F| > 2\ \sigma\ |F|$.

$R_{sym} = \Sigma|I-\langle I\rangle|/\Sigma I$, where I = observed intensity, $\langle I\rangle$ = average intensity obtained from multiple observations of symmetry related reflections. $R_{iso} = \Sigma||F_{PH}| - |F_P||/\Sigma|F_P|$, where $|F_P|$ = protein structure factor amplitude, $|F_{PH}|$ = heavy-atom derivative structure factor amplitude. Phasing power = rms ($|F_H|/E$), where $|F_H|$ = heavy-atom structure factor amplitude, E = residual lack of closure. $R_c = \Sigma||F_{PH} \pm |F_P| - |F_{H,calc}|\ |\ /\Sigma|\ |F_{PH} \pm |\ F_P|\ |$, with the sum taken over all centric reflections. $R_{free}$ was calculated with 5% of data, $R_{work}$ calculated with the remaining 95% of reflections.

subunits are asymmetric, as 2,550 Å$^2$ (31% hydrophobic) are buried in contacts to its left neighbor and 2,190 Å$^2$ (50% hydrophobic) in contacts to its right neighbor. The contacts involve mainly the equatorial (1,490 Å$^2$, 56% hydrophobic) and the apical (2,190 Å$^2$, 38% hydrophobic) domains (Figure 3B). There are irregularly shaped side windows between the intermediate and the apical domains. These measure approximately 25 Å $\times$ 10 Å between C$\alpha$ atoms to the right side of an $\alpha$ subunit and 20 Å $\times$ 6 Å to the left side. A total fraction of 75% of the surface area of each $\alpha$ and $\beta$ subunit remains solvent exposed, only 18% of which is hydrophobic.

The intra-ring contacts between the equatorial domains comprise a $\beta$ sheet between strands S2 and S3 of one monomer, the stem loop (Braig et al., 1994; Boisvert et al., 1996), and S1 and S25 of an adjacent subunit. In addition, the N-terminal part of helix H6 interacts with the loop region between helix H2 and strand S2 flanking the nucleotide-binding site, and helices H4 and H18 interact with both the neighboring equatorial and intermediate domains. The intermediate domain, tilted toward the equatorial domain, forms the upper part of the nucleotide-binding site on top of the equatorial domain and is linked via its hinge-distal region to the nucleotide-binding site at the C terminus of helix H4 of the adjacent subunit. Turn segments between helices H7 and H8 and between strands S7 and S8, together with a turn between strand S20 and helix H14, approach helices H4,

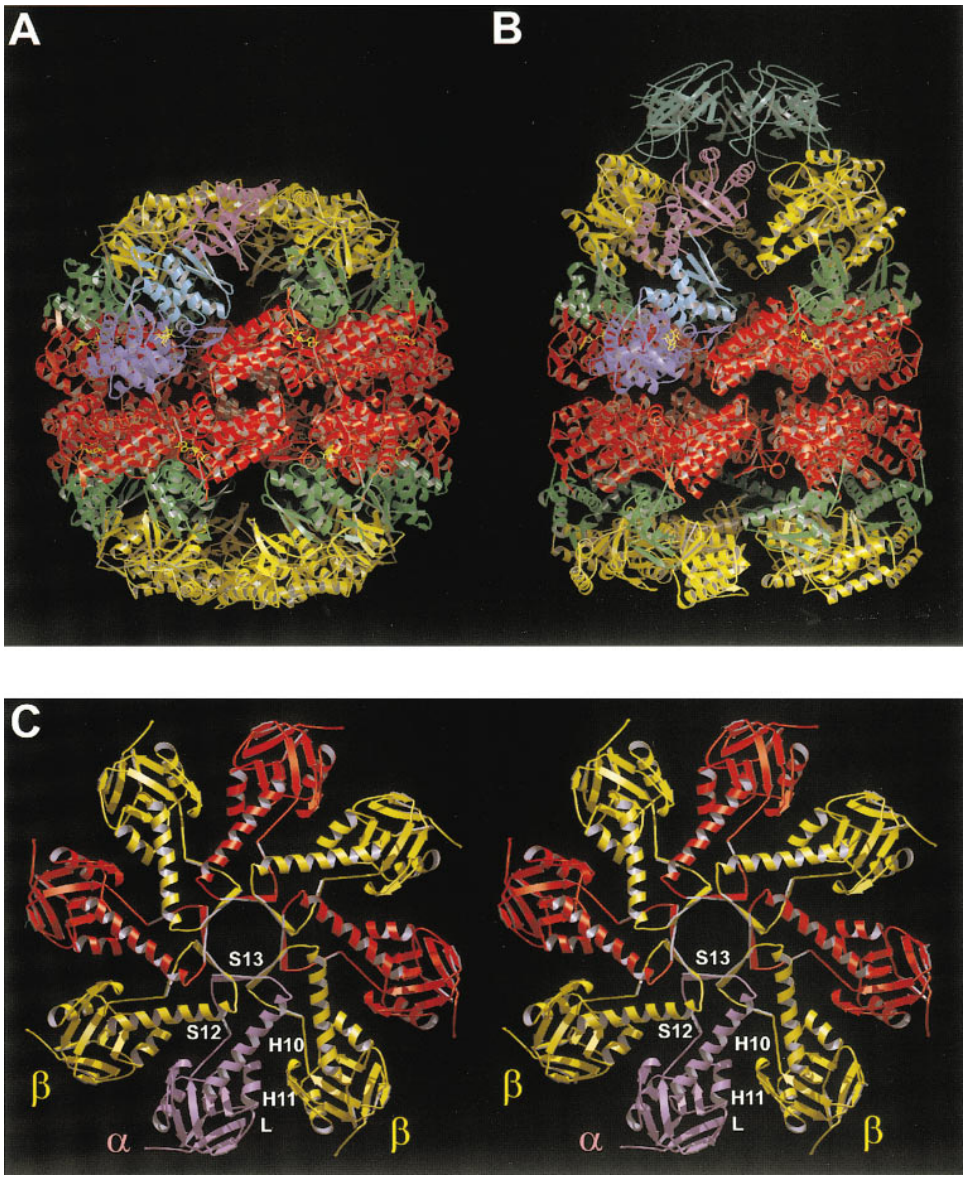


Figure 1. General Architecture of Chaperonins

(A) Side view of the hexadecameric thermosome structure.

(B) Side view of the asymmetric GroEL-GroES-$(ADP)_7$ complex (Xu et al., 1997a).

Domains are colored in red (equatorial), green (intermediate), and yellow (apical). Within each complex domains of aligned subunits are highlighted in blue (equatorial), light blue (intermediate), and violet (apical). Bound ADP is drawn in yellow.

(C) Top view of the thermosome α (red/violet) and β (yellow) apical domains. β strands S12 and S13 and the N-terminal half of helix H10 (lid segments) form the lid domain that seals off the central chamber. Helices H10 and H11 and loop L topologically correspond to helices H and I and the loop connecting β strands 6 and 7 in GroEL that are involved in substrate and/or GroES binding.

Figures 1A, 1B, 3, 5, and 6A were generated using BOBSCRIPT (Esnouf, 1997) and RASTER3D (Bacon and Anderson, 1988; Merrit and Murphy, 1994). Figure 1C was prepared with MOLSCRIPT (Kraulis, 1991) as modified by D. Peisach and E. Peisach and with POVRAY.

H6, and H18 in the adjacent equatorial domain. A third stretch of sequence, the flip loop between H4 and H5, interacts with these loops at the nucleotide-binding site (Figure 3B). Apart from the tight interactions within the lid segments, there is only one major contact site between adjacent apical domains of α and β subunits: helices H11 and H13 of adjacent subunits interact at the top of the particle. No other part of the apical domain makes any contacts to neighboring subunits, except a loop in the β subunit (residues β354 and β355) that interacts with Gln-α88, thereby linking the nucleotide-binding region to the apical domain.

**Inter-ring Contacts**

Whereas the intra-ring contacts between the equatorial domains are conserved between group I and group II

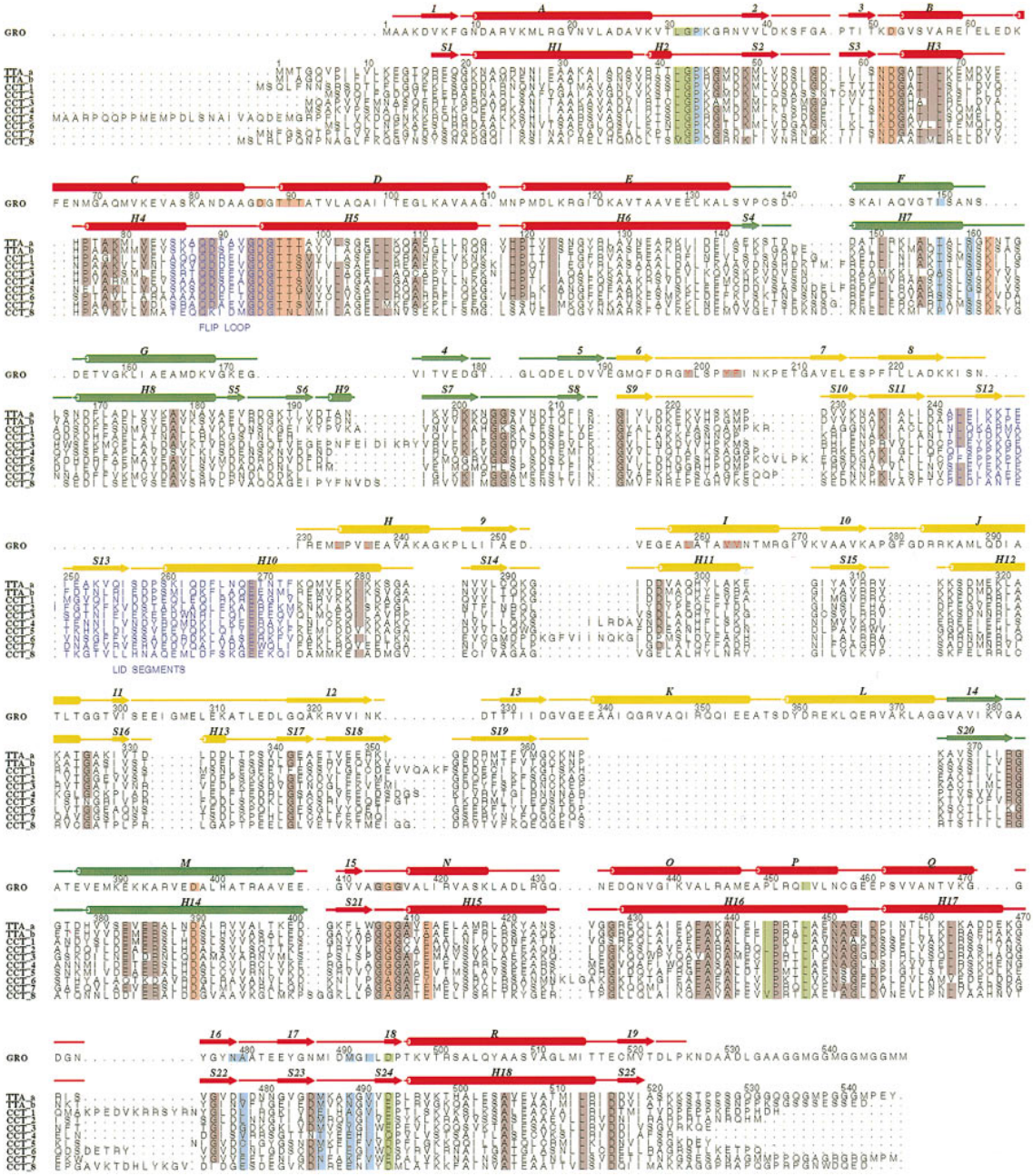


Figure 2. Alignment of Chaperonin Sequences

Structure-based alignment of the sequences of GroEL, thermosome α and β subunits, and the eight CCT subunits of *S. cerevisiae*. The secondary structural elements of the thermosome were assigned by the program DSSP (Kabsch and Sander, 1983) and adjusted after visual inspection. The GroEL secondary structure assignment was taken from Xu et al. (1997a). Color coding corresponds to Figures 1A and 1B. Residues contributing to the flip loop and apical lid segments are depicted in blue. Residues participating in nucleotide binding are highlighted according to interactions with the nucleobase (light blue), ribose (green), or phosphate groups (pink). Amino acids that are conserved in at least eight out of the ten group II chaperonin sequences are shaded in gray. Substrate binding residues in GroEL (Fenton et al., 1994) are depicted in red and shaded in gray. Figure produced using ALSCRIPT (Barton, 1993).

chaperonins, the inter-ring contacts are different (Figures 3C and 3D). In GroEL, the 2-fold axis runs along the right and left edge of the upper subunit, relating helices D and Q to those of two different subunits in the lower ring (Figure 3D). In the thermosome, the 2-fold axis runs along the center of the upper subunit, generating α-α and β-β pairs (Figure 3C). The upper α subunit contributes residues from the C terminus of helix H5 (Thr-112, Asp-115, and Gln-116) and from the N terminus of helix H16 (Arg-429 and Leu-421) to the contact at the left side. The lower α subunit contributes residues from the C terminus of helix H16 (Arg-446 and Asp-450) and N terminus of helix H17 (Asp-455, Pro-456, Ile-457, and Asn-458).

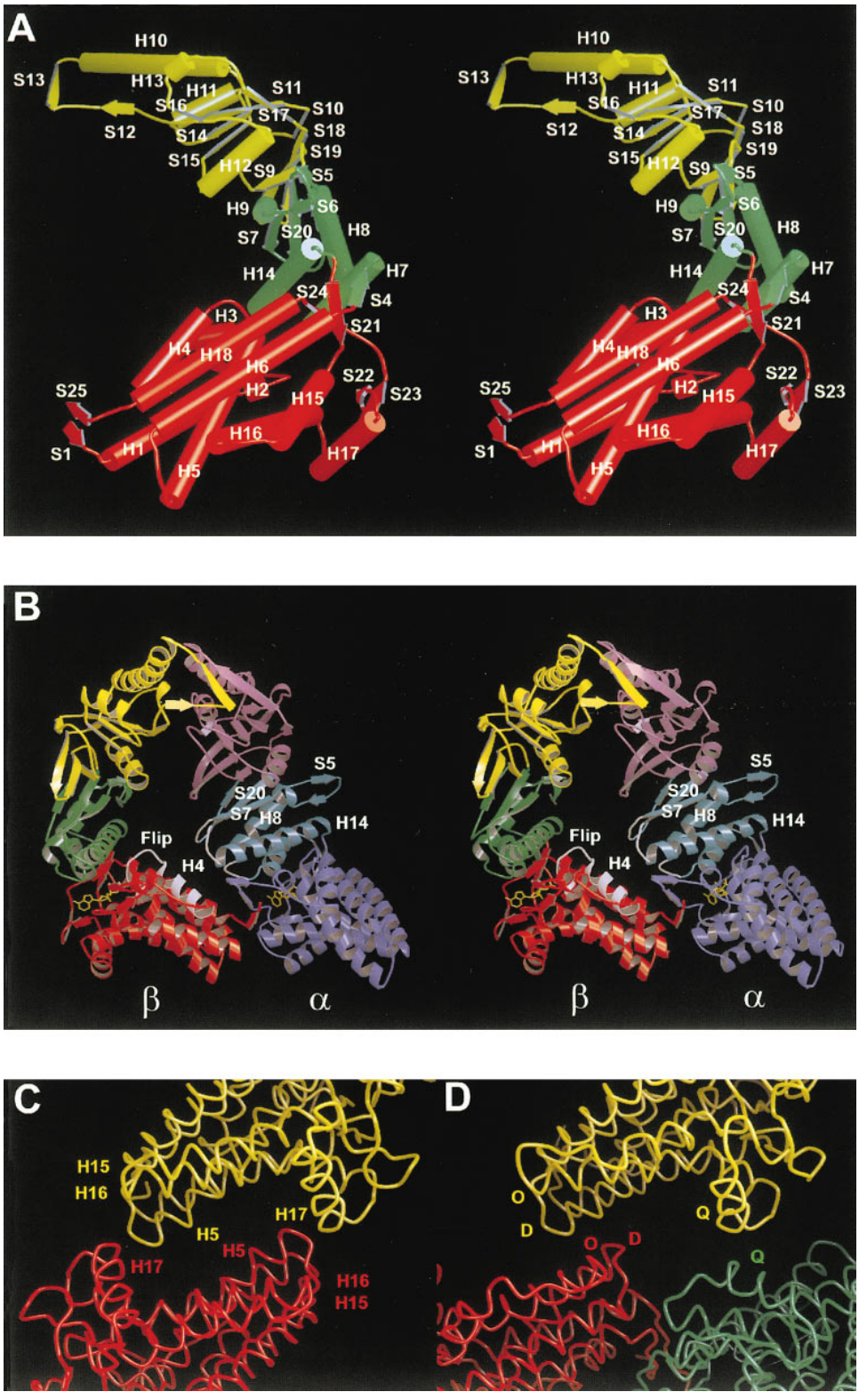


Figure 3. Subunit Structure and Contacts

(A) Schematic drawing of the secondary structural elements of a thermosome α subunit. Helices and strands are labeled and colored as in Figure 2. With respect to Figure 1A the view corresponds to a 90° rotation around the pseudo 8-fold axis.
(B) Intra-ring contacts between two thermosome subunits as viewed from the inside of the particle. The α and β monomers are color coded as in Figure 1A, and the bound nucleotides are shown in yellow.
(C) Inter-ring contacts between two thermosome α subunits related by 2-fold symmetry.
(D) GroEL inter-ring contacts. One subunit in the upper ring is related to two subunits in the lower ring by 2-fold axes at the right and left edge of the upper subunit.

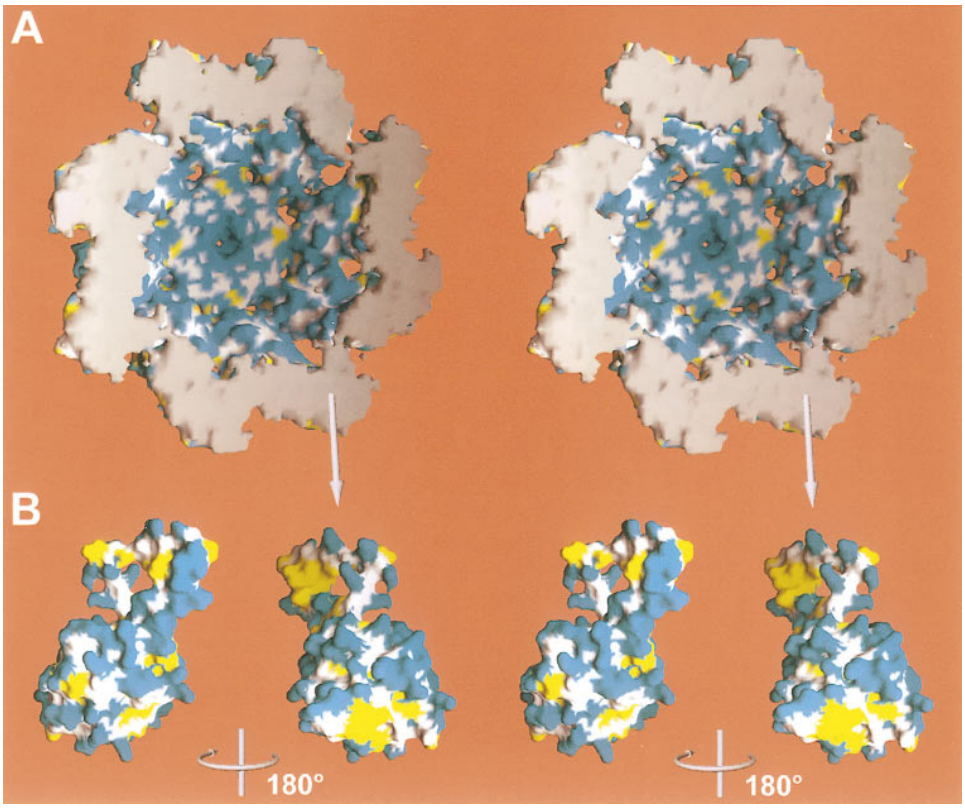


Figure 4. The Folding Chamber

(A) Surface representation of the internal cavity of the thermosome. The solvent-exposed surface of the intermediate and apical domains is colored according to polarity: backbone atoms in white, polar and charged side chain atoms in turquoise, hydrophobic side chain atoms in yellow. Solvent-excluded atoms visible at the cut open plane are in gray.

(B) Surface representation of the apical domain of a thermosome $\alpha$ subunit color coded according to hydrophobicity. The orientation on the left corresponds to a view from the outside as shown in Figure 1C for the violet domain. The domain in the right panel has been rotated by 180°, which corresponds to the view from the inside as in (A). Generated using GRASP (Nicholls et al., 1993).

The buried surface area at the inter-ring interface between $\alpha$ subunits is 710 Å$^2$ (25% hydrophobic) and 480 Å$^2$ (38% hydrophobic) between $\beta$ subunits. The buried surface area is greater between $\alpha$ subunits mainly because of an additional contact formed by a symmetric salt bridge between Arg-25 and Glu-29 in the H1 helix from each subunit. The corresponding residues in the $\beta$ subunit (Lys-$\beta$24, Glu-$\beta$28) are not defined by electron density.

**The Lid Domain**

A total of 33 residues from each subunit, comprising $\beta$ strands S12 and S13 and most of the N-terminal part of helix H10, protrude toward the pseudo 8-fold molecular axis at both ends of the particle and block the entrance to the central cavity by forming the lid domain (Figures 1C and 4A). Eight S13 $\beta$ strands form a circularly closed parallel $\beta$ sheet, forming a central pore with a diameter of 19 Å between C$\alpha$ atoms. The triangle of S12, S13, and the N-terminal part of H10 packs against the equivalent structural unit of two neighbors. Each subunit contributes nine hydrophobic residues and one Thr residue to a core of almost exclusively hydrophobic character (Figure 4B). One-third of all lid segment residues, including all hydrophobic residues, are buried completely in this core. These tight interactions within the lid domain fix the apical domains of the thermosome in a conformation equivalent to that of the *cis*-ring of the GroEL-GroES complex. At the lid domain, seven hydrophilic residues and one Ile residue from each subunit are exposed toward the cavity (Figure 4A).

**The Central Cavity**

The thermosome encloses a central cavity with a height of 115 Å along the pseudo 8-fold axis. The inner diameter decreases from 86 Å between opposing equatorial domains to 54 Å at the top of the chamber, which is closed by the lid domain (Figure 4A). The total volume of the chamber is 325,000 Å$^3$. However, taking into account a total of 336 disordered residues from the N and C termini of all 16 subunits and assuming a partial specific volume of 1.7 Å$^3$ per dalton leaves a total volume of 130,000 Å$^3$ within each ring. The effective height of each of the resulting chambers is approximately 45 Å. The disordered residues may serve as a flexible septum as has been shown for GroEL, where they appear to block transit between both chambers (Chen et al., 1994). The volume of the thermosome central cavity is significantly smaller than that of the *cis*-cavity of the GroEL-GroES

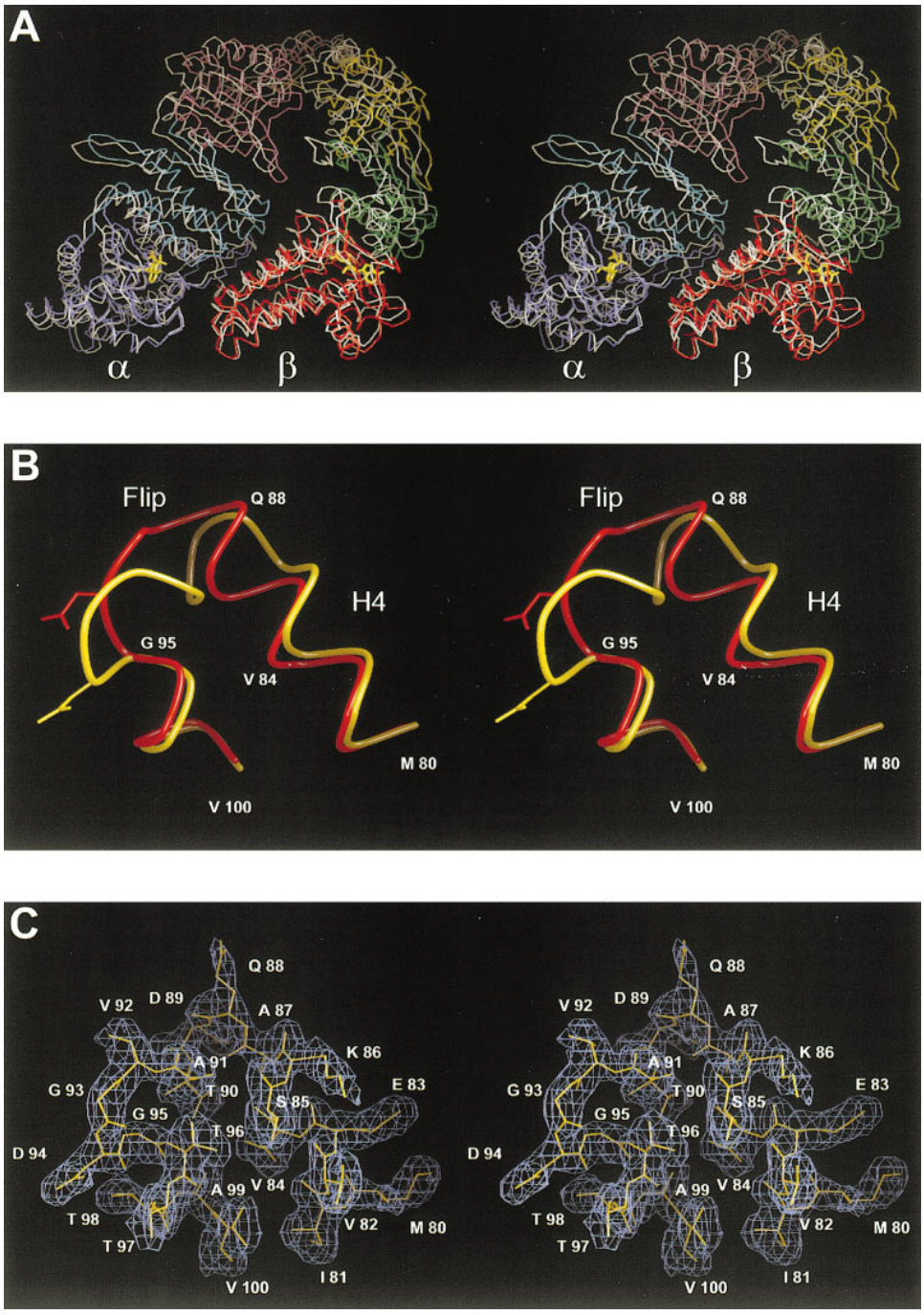


Figure 5. Effects of Nucleotide Binding

(A) Superposition of Cα atoms of the thermosome αβ-dimer crystallized in the absence of nucleotide (crystal form NATI), color coded as in Figure 1A, and in the presence of 3 mM Mg-ADP (crystal forms MADC1), shown in gray. In crystal form MADC2 two αβ-dimers are asymmetric, related by 2-fold noncrystallographic symmetry with an rmsd value of 0.14 Å for a 180° rotation. A rotation of 4.5° around the molecular 4-fold axes results in an rmsd value of 0.35 Å (α subunit) and 0.39 Å (β subunit) for Cα atoms of the secondary structure elements of crystal form MADC1. Domain motions can be described by an outward tilt of the equatorial domain (6.1° in α, 7.1° in β) maintaining the contact surface followed by an upward rotation of the intermediate domain around the equatorial-intermediate pivot (1.9° in α, 3.6° in β) and a clockwise rotation around the intermediate-apical hinge (4.2° in α, 5.5° in β).

(B) Schematic drawing of the α-flip loop rearrangement. In the ligand-free structure (yellow), Asp-94 protrudes into the nucleotide-binding site. Upon nucleotide binding it is displaced (red), and the loop rearranges by elongation of helix H4.

(C) Electron density map of the thermosome α-flip loop as seen in the nucleotide-free structure. The map was calculated with $2|F_o|-|F_c|$ coefficients and model phases; contour level is 1σ.

complex (175,000 Å$^3$) but larger than that of the corresponding *trans*-cavity (85,000 Å$^3$) (Xu et al., 1997a).

Access to the central cavity is possible only through irregularly shaped side windows (Figure 1A), which are too small to allow entry and exit of intact substrate proteins, when van der Waals radii of side chains are taken into account. The same applies for the opening in the center of the lid domain (Figure 1C). The central chamber is large enough to accommodate a medium-sized protein with a molecular weight of about 50 kDa. The atomic model of the 44 kDa protein actin (Kabsch et al., 1990), a substrate for the eukaryotic homolog CCT, can be accommodated inside the central chamber of the thermosome structure in accordance with the view that substrates are released in a native or near-native conformation in a productive folding cycle. The reduced volume of the thermosome central cavity, which is only about 74% of the *cis*-GroEL-GroES cavity, suggests a decreased upper size limit for group II chaperonins compared to group I chaperonins.

**Nucleotide Binding**

Two Mg-ADP-bound crystal forms of the thermosome confirm the location of the nucleotide-binding site on top of the equatorial domain and show a domain arrangement that is distinct from the unliganded form (Figure 5A). Domain motions are allowed by pivots connecting the equatorial, intermediate, and apical domains and result in a displacement of up to 4.8 Å on the outer surface of the apical domains. The lid domain, however, remains unchanged.

Nucleotide binding induces a major rearrangement in the loop region connecting helices H4 and H5 (Figures 3B and 5B). Within this flip loop, which is well defined in the electron density map (Figure 5C), Asp-94 of the GDGTTT motif occupies the triphosphate-binding site in the absence of nucleotide and is displaced by the phosphates. Residues 89–98 are shifted toward the hinge-distal portion of the neighboring intermediate domain and force residues 85–88 to change from a relaxed loop structure to a helical conformation. In GroEL, nucleotide binding appeared to induce only two small structural changes (Boisvert et al., 1996). Helix C, which corresponds to helix H4 in the thermosome (Figure 3B), is axially translated. Secondly, the stem loop ($\beta$2/$\beta$3) moves, which provides a contact to the N and C termini of the neighboring subunit. No such movements were observed in the thermosome structure.

Soaking experiments conducted with ADP, ATP, Mg-ADP, and Mg-ATP-$\gamma$-S (Table 1) showed that the nucleotide-binding site is still accessible in a domain arrangement where the intermediate domain is clamped onto the equatorial domain and access to the active site is only provided through a narrow channel from the outside of the particle. This is in contradiction to GroEL, where it has been postulated that ADP is nonexchangeably bound in the domain orientation of the GroEL-GroES *cis*-ring (Xu et al., 1997a).

**Transition State of ATP Hydrolysis**

Nucleotide-induced domain rearrangements are characteristic for the folding cycle in group I chaperonins (Roseman et al., 1996) and modulate substrate affinity. Conformational changes induced by Mg-ATP have been observed for CCT by electron microscopy (Gao et al., 1992) that alter the side-view projection profile from a barrel-shaped outline toward that of two stacked, truncated cones (Marco et al., 1994a). It has been shown that the Mg-ADP-bound form of CCT is capable of binding unfolded target proteins, whereas the Mg-ADP-beryllium-fluoride complex, which mimics the transition state of ATP hydrolysis and closely resembles the Mg-ATP-bound form, completely fails to bind unfolded target proteins (Melki and Cowan, 1994). These experiments indicate the existence of distinct molecular states of CCT that differ with respect to the accessibility of the substrate-binding regions. GroEL functions in an analogous fashion.

The central chamber of the thermosome closely resembles the *cis*-chamber of the asymmetric GroEL-GroES complex, which was identified as the folding-active conformation (Hayer-Hartl et al., 1995; Mayhew et al., 1996; Weissman et al., 1996) with respect to its hydrophilicity and domain arrangement. This suggests that the closed conformation observed in the present study represents the ATP-stabilized form that is not capable of substrate binding. This was corroborated by a soaking experiment where the transition state analog Mg-ADP-$AlF_3$ was bound to the active site of the ATPase (Figure 6A). In that complex one fluorine contributes to the coordination sphere of the Mg; the remaining two fluorines form hydrogen bonds to Thr-96 and Thr-97, respectively. The water molecule at the apex of the trigonal bipyramid is fixed by hydrogen bonds to Asp-63 of the equatorial domain and Asp-390 (Asp-398 in GroEL) of the intermediate domain with a length of 2.8 Å each (Figure 6B). The importance of Asp-398 for ATPase activity in GroEL has already been shown (Rye et al., 1997), and the analogous residues Asp-63 (thermosome) and Asp-52 (GroEL) adopt nearly identical orientations. This suggests a common mechanism of ATP hydrolysis for group I and group II chaperonins (Figure 6C) involving residues from both the equatorial and intermediate domains. In addition, it supports a model of nucleotide-induced conformational changes as advanced for group I chaperonins (Xu et al., 1997a). The $\gamma$-phosphate of ATP stabilizes the folding-active GroEL-GroES *cis*-ring arrangement by providing a strong contact to the intermediate domain. This contact is observed in the thermosome for Asp-390 in the Mg-ADP-$AlF_3$ structure. Hydrolysis of ATP obliterates this contact and the metastable arrangement relaxes upon binding of ATP to the *trans*-ring mediated by negative allosteric signaling between both rings (Rye et al., 1997).

The high-salt conditions used for crystallization may have favored the closed conformation of the thermosome over a more open structure with exposed hydrophobic patches. The closed conformation may, therefore, differ from the Mg-ADP-bound solution state under physiological conditions. A similar observation was made for GroEL cocrystallized with Mg-ATP-$\gamma$-S (Boisvert et al., 1996), which does not reflect the solution state (Roseman et al., 1996). Clearly, further electron microscopy studies are needed for definitely correlating the observed thermosome conformation to a functional state of the folding cycle.

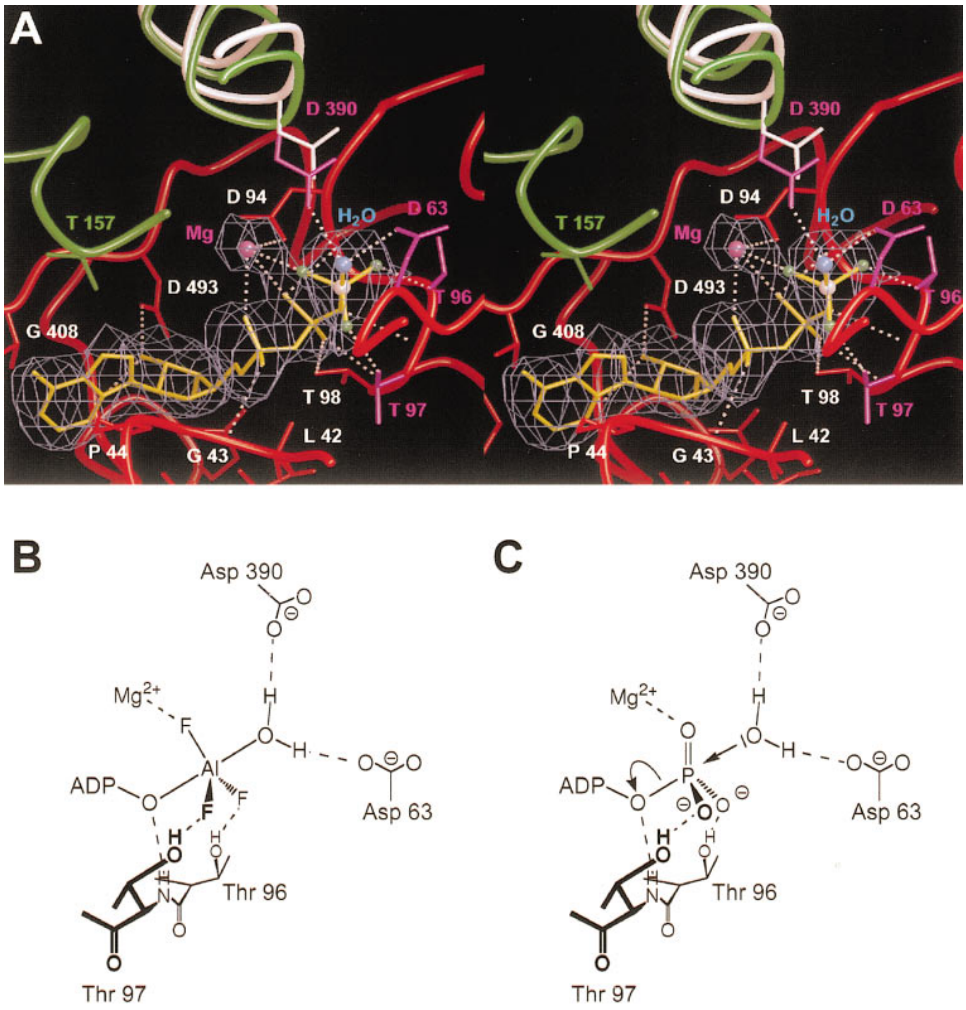


Figure 6. Active Site Geometry and Proposed Mechanism of ATP Hydrolysis

(A) Stereoview of an $|F_o|-|F_c|$ omit map of the electron density centered on the Mg-ADP-aluminium fluoride of the α subunit soaked into the nucleotide-binding site of the thermosome and contoured at 2σ. Fluoroaluminate can bind to the β-phosphate of ADP either as $AlF_4^-$ (Sondek et al., 1994) or $AlF_3$ (Xu et al., 1997b). The electron density adjacent to the β-phosphate was best interpreted with an $AlF_3$ molecule. One fluorine atom (green) contributes to the coordination sphere of Mg (purple); the remaining two atoms are hydrogen bonded to Thr-96 and Thr-97. A water molecule (blue) at the apex of the trigonal bipyramid forms hydrogen bonds to Asp-63 of the equatorial domain and to Asp-390 of the intermediate domain. No other contact between the intermediate domain and the γ-moiety was observed. The Cα atom of Asp-390 approaches the $AlF_3$ group by 1.5 Å, as compared with the Mg-ADP complex (helix H14 shown in white) prepared by soaking. The $AlF_3$ moiety was fully occupied in the α subunit (compared to the peak height of the α- and β-phosphates) but had a lower occupancy in the β subunit (approximately 55% as estimated from the relative peak heights of $AlF_3$) where the shift of helix H14 was not observed.

(B) Schematic drawing of the $AlF_3$ environment.

(C) Proposed mechanism of ATP hydrolysis. In analogy to the observed binding mode of the $AlF_3$ group, the γ-phosphate ion is stabilized in its trigonal-bipyramidal configuration by interactions with the conserved threonines and by coordination to the magnesium ion. The attacking water nucleophile is held and polarized by hydrogen bonds to the side chains of Asp-63 and Asp-390, and collapse of that pentavalent intermediate yields a terminal β-phosphate and a free orthophosphate.

**Substrate Binding**

The substrate-binding site of GroEL has been mapped to one side of the apical domain, which places hydrophobic residues in the cleft between helices H and I and in the loop connecting β strands 6 and 7 (Fenton et al., 1994). This region is exposed toward the central cavity in the substrate-binding *trans*-ring of the GroEL-GroES complex, but it is buried in contacts to a neighboring subunit or to GroES in the folding-active *cis*-ring (Xu et al., 1997a). A structure-based sequence comparison (Figure 2) shows hydrophilic character for this region in the group II chaperonins (Klumpp et al., 1997). It comprises the C-terminal portion of helix H10, helix H11, and the loop connecting β strands S9 and S10 (Figure 2). This loop (denoted L) is buried in a contact to its right-hand neighbor (Figure 1C). The cleft between helices H10 and H11 is completely exposed to the outside of the thermosome. In the folding-active *cis*-ring of the

GroEL-GroES complex, the hydrophobic surface patches of the corresponding helices H and I, involved in substrate binding, are shielded by bound GroES. In the thermosome, the decreased hydrophobicity of that region suggests a different mode of substrate binding because it remains partially exposed in the closed conformation, as a GroES-like cochaperonin does not exist. If the substrate-binding regions were conserved between group I and group II chaperonins, the regions mapped in GroEL could contribute electrostatic charge to the recognition pattern. The importance of both hydrophobicity and charge in substrate binding have been demonstrated in GroEL (reviewed by Coyle et al., 1997).

However, hydrophobic interactions have been implicated in substrate binding in both group I and group II chaperonins (Guagliardi et al., 1994; Dobrzynski et al., 1996). Apart from the contact surface between intermediate and apical domains, contiguous hydrophobic surface patches are present only in the lid segments forming the hydrophobic core of the lid domain (Figure 4B). These tight interactions are not strong enough, however, to stabilize higher aggregates of isolated apical domains, which crystallize as dimers and make extensive contact between hydrophobic patches of the lid segments (Klumpp et al., 1997) unrelated to the orientation in the intact particle. This demonstrates the stability of the apical domain as an isolated entity, and the transition of the open triangular structure of β strands S12 and S13 to a more compact α helix comprising residues 247–255 may indicate the provision of alternative contacts upon domain rearrangement.

Electron microscopy of α-only thermosomes under low-salt conditions in the absence of nucleotide (Nitsch et al., 1997) showed a rectangular projection map rather than a spherical outline that is observed in the crystal structure of the thermosome, in line with observations made on the CCT system (Marco et al., 1994a). An open form of the thermosome can be modeled by analogy with the substrate-binding *trans*-ring of the GroEL-GroES complex (Braig et al., 1994; Xu et al., 1997a; data not shown). In the thermosome this necessitates a counter clockwise rotation of the apical domains (Figure 1C). In this conformation, helix H10 of the lid segment would be stripped off the β strands S12 and S13 of the right-hand neighbor and thus would form the upper edge of the central channel. The remaining residues comprising β sheets S12 and S13 would face the C-terminal half of helix H10 of the left-hand neighbor, where packing would be improved by a contraction to a helix as observed for an isolated apical domain (Klumpp et al., 1997). In this scenario the lid insertions could provide hydrophobic residues (Ile-250, Val-254, Pro-259, Ile-262, and Leu-266) on the central channel capable of substrate binding. The lid segment might function as an iris-type aperture with a dual role for both closing the cage and binding substrate. However, mutagenesis studies will be necessary to map the substrate-binding site of group II chaperonins.

## Experimental Procedures

### Protein Preparation and Crystallization

*T. acidophilum* cells were grown at 56°C at pH 2.0 in a 300 l fermenter (Bioengineering, Switzerland) containing 255 l of medium (Darland and Brock, 1971) supplemented with 1% glucose and 0.1% yeast extract. After reaching the late logarithmic growth phase, cells were harvested in a flow-through centrifuge (Padberg, Germany) and frozen in liquid nitrogen. The yield was between 80 and 120 g wet weight cells. For lysis, 10 g of cells were suspended in 100 ml of buffer A (20 mM Tris-HCl, 1 mM EDTA, 0.02% w/v $NaN_3$ [pH 7.5]) containing 3 mg DNase I, 1 mg RNase A, 0.1 mM leupeptin, 0.5 mM PMSF, and 40 mM NaCl. Cell disruption was performed by adjusting the pH to 7.5 with 1 M Tris and subsequent brief sonication. After ultracentrifugation (175,000 × g, 1 hr) the supernatant was applied to a DE52 column (200 ml; Whatman) equilibrated in 40 mM NaCl/buffer A. The column was washed with 40 mM NaCl in buffer A, and proteins were eluted with a linear gradient of 40–180 mM NaCl in 1000 ml of buffer A. Fractions were analyzed by SDS-PAGE (Schägger and von Jagow, 1987), and pooled fractions (80–120 mM NaCl) were applied to a hydroxyapatite column (100 ml; MacroPrep ceramic hydroxyapatite 40 μm, BioRad) equilibrated in 200 mM buffer B ($KH_2PO_4/K_2HPO_4$ [pH 7.5]). Contaminants were removed by rinsing with 200 mM buffer B, and elution was done with a 1000 ml linear gradient of 200–400 mM buffer B. Fractions were pooled according to SDS-PAGE analysis (240–300 mM potassium phosphate) and were diluted 10-fold with buffer A and loaded onto a Q-Sepharose column (200 ml; Pharmacia) equilibrated in buffer A. The column was washed with 50 mM NaCl in buffer A, and proteins were eluted with a linear gradient of 50–250 mM NaCl in 1000 ml of buffer A. Pooled fractions (130–170 mM NaCl) were dialyzed against buffer C (20 mM Tris-HCl, 0.02% $NaN_3$ [pH 7.5]) for 12 hr, concentrated by ultrafiltration, and used immediately for crystallization. The yield was about 8 mg of pure thermosome. All preparation steps were performed at 4°C.

Crystals were grown at 20°C using the sitting drop vapor diffusion method. Five microliters of a solution containing 10 mg/ml thermosome in buffer C were mixed with 2.5 μl of precipitant comprising 2 M ammonium sulphate and 0.1 M sodium acetate (pH 5.6) and equilibrated against 5 ml of a corresponding reservoir solution. Crystals appeared within 2–3 days and reached a size of about 0.5 × 0.5 × 0.4 $mm^3$ within two weeks. They belong to spacegroup I422 or I4 with unit cell dimensions shown in Table 1 containing two or four monomers per asymmetric unit, respectively. SDS-PAGE analysis of redissolved crystals showed that the protein composition was indistinguishable from that found in the mother liquor. Cocrystallization and soaking experiments were performed as indicated in Table 1.

### Data Collection and Processing

Native data sets were collected on beamline BW6 at DESY, Hamburg, using a Mar research imaging plate system with synchrotron radiation of λ = 1.1 Å. Nucleotide-bound complexes obtained by cocrystallization yielded two different crystal forms; synchrotron data were merged from 30 (NATI), 3 (MADC1), or 27 (MADC2) different crystals. All complexes obtained by soaking experiments (heavy atom derivatives and nucleotide complexes) were measured in-house using a Mar research imaging plate detector mounted on a Rigaku rotating anode X-ray generator, operating at 50 kV and 100 mA. Measured intensities were integrated with MOSFLM (Leslie, 1991) and scaled and merged using the CCP4 program suite (Collaborative Computational Project, 1994).

### Phasing, Model Building, and Refinement

Heavy atom positions were located with SHELX (Sheldrick et al., 1993) and confirmed by difference Fourier syntheses. Heavy atom parameters were refined and phases calculated with MLPHARE (Collaborative Computational Project, 1994). MIR phases were improved by cycles of solvent flattening using DM (Cowtan, 1994) and yielded a 4.0 Å electron density map that was interpretable in terms of polypeptide main-chain connectivity. A model of GroEL (Boisvert et al., 1996) was truncated to polyalanine, and the equatorial and intermediate domains were fitted into the electron density as rigid bodies using FRODO (Jones, 1978). After phase combination and solvent flattening, the apical domains could be fitted into the new electron density map, and subsequent phase combination allowed corrections of the main-chain tracing. After a further round of phase

combination, an electron density map at 2.6 Å was calculated with $2|F_o|-|F_c|$ coefficients. The α and β subunits were identified according to characteristic stretches of electron density, and the model was completed during iterative rounds of model building and refinement (X-PLOR: Brünger, 1992) using Engh and Huber parameters (Engh and Huber, 1991). In the final stages, restrained individual temperature factors were refined. No solvent molecules have been included in the model. Refinement statistics are summarized in Table 1. A Ramachandran plot performed with PROCHECK (Laskowski et al., 1993) shows a residue distribution of the ligand-free complex of 90.8% and 8.4% within the core and allowed regions, respectively.

For analysis of nucleotide binding, the native structure was refined against the corresponding datasets. Electron density maps calculated with $2|F_o|-|F_c|$ coefficients clearly revealed the bound nucleotides. The models were completed and adjusted iteratively with successive rounds of refinement. In the case of the I4 symmetric crystal form, electron density maps were averaged 2-fold with MAIN (Turk, 1992), and 2-fold noncrystallographic restraints were imposed on coordinate and temperature factor refinement (Table 1). Solvent accessible surfaces were calculated using X-PLOR with a probe radius of 1.4 Å, and the volume of the central cavity was calculated with VOIDOO (Kleywegt and Jones, 1994) using default parameters.

**Acknowledgments**

We thank F.-U. Hartl and A. Chapin Rodriguez for critical reading of the manuscript, H. D. Bartunik for support with synchrotron data collection, and Kerstin Roth for excellent technical assistance. Supported in part by Fonds der Chemischen Industrie (L. D.).

Received December 18, 1997; revised February 17, 1998.

**References**

Andrä, S., Frey, G., Nitsch, M., Baumeister, W., and Stetter, K.O. (1996). Purification and structural characterization of the thermosome from the hyperthermophilic archaeum Methanopyrus kandleri. FEBS Lett. *379*, 127–131.

Azem, A., Kessel, M., and Goloubinoff, P. (1994). Characterization of a functional $GroEL_{14}(GroES_7)_2$ chaperonin hetero-oligomer. Science *265*, 653–656.

Bacon, D.J., and Anderson, W.F. (1988). A fast algorithm for rendering space-filling molecule pictures. J. Mol. Graph. *6*, 219–220.

Barton, G.J. (1993). ALSCRIPT. A tool to format multiple sequence alignments. Protein Eng. *6*, 37–40.

Boisvert, D.C., Wang, J., Otwinowski, Z., Horwich, A.L., and Sigler, P.B. (1996). The 2.4 Å crystal structure of the bacterial chaperonin GroEL complexed with ATP-γ-S. Nature Struct. Biol. *3*, 170–177.

Braig, K., Otwinowski, Z., Hegde, R., Boisvert, D.C., Joachimiak, A., Horwich, A.L., and Sigler, P.B. (1994). The crystal structure of the bacterial chaperonin GroEL at 2.8 Å. Nature *371*, 578–586.

Brünger, A. (1992). X-PLOR Version 3.1. A System for Crystallography and NMR (New Haven, CT: Yale University Press).

Chen, S., Roseman, A.M., Hunter, A.S., Wood, S.P., Burston, S.G., Ranson, N.A., Clarks, A.R., and Saibil, H.R. (1994). Location of a folding protein and shape changes in GroEL-GroES complexes imaged by cryo-electron microscopy. Nature *371*, 261–264.

Cheng, M.Y., Hartl, F.-U., Martin, J., Pollock, R.A., Kalousek, F., Neupert, W., Hallberg, E.M., Hallberg, R.L., and Horwich, A.L. (1989). Mitochondrial heat-shock protein hsp60 is essential for assembly of proteins imported into yeast mitochondria. Nature *337*, 620–625.

Collaborative Computational Project, N. (1994). The CCP4 suite: programs for protein crystallography. Acta Crystallogr. *D50*, 760–763.

Cowtan, K. (1994). DM: an automated procedure for phase improvement by density modification. Joint CCP4 and ESF-EACBM Newsletter Protein Crystallogr. *31*, 34–38.

Coyle, J.E., Jaeger, J., Gross, M, Robinson, C.V., and Radford, S.E. (1997). Structural and mechanistic consequences of polypeptide binding by GroEL. Folding and Design *2*, R93-R104.

Darland, G., and Brock, T.D. (1971). Bacillus acidocaldarius sp. nov., an acidophilic thermophilic spore-forming bacterium. J. Gen. Microbiol. *76*, 9–15.

Dobrzynski, J.K., Sternlicht, M.L., Farr, G.W., and Sternlicht, H. (1996). Newly synthesized β-tubulin demonstrates domain-specific interactions with the cytosolic chaperonin. Biochemistry *35*, 15870–15882.

Ellis, R.J., and Hartl, F.-U. (1996). Protein folding in the cell: competing models of chaperonin function. FASEB J. *10*, 20–26.

Engel, A., Hayer-Hartl, M.K., Goldie, K.N., Pfeifer, G., Hegerl, R., Müller, S., da Silva, A.C.R., Baumeister, W., and Hartl, F.-U. (1995). Functional significance of symmetrical versus asymmetrical GroEL-GroES chaperonin complexes. Science *269*, 832–836.

Engh, R.A., and Huber, R. (1991). Accurate bond and angle parameters for X-ray protein structure refinement. Acta Crystallogr. *A47*, 392–400.

Esnouf, R.M. (1997). An extensively modified version of MolScript that includes greatly enhanced coloring capabilities. J. Mol. Graph. *15*, 132–134.

Ewalt, K.L., Hendrick, J.P., Houry, W.A., and Hartl, F.U. (1997). In vivo observation of polypeptide flux through the bacterial chaperonin system. Cell *90*, 491–500.

Farr, G.W., Scharl, E.C., Schumacher, R.J., Sondek, S., and Horwich, A.L. (1997). Chaperonin-mediated folding in the eukaryotic cytosol proceeds through rounds of release of native and nonnative forms. Cell *89*, 927–937.

Fenton, W.A., and Horwich, A.L. (1997). GroEL-mediated protein folding. Protein Sci. *6*, 743–760.

Fenton, W.A., Kashi, Y., Furtak, K., and Horwich, A.L. (1994). Residues in chaperonin GroEL required for polypeptide binding and release. Nature *371*, 614–619.

Frydman, J., Nimmesgern, E., Erdjument-Bromage, H., Wall, J.S., Tempst, P., and Hartl, F.-U. (1992). Function in protein folding of TRiC, a cytosolic ring complex containing TCP-1 and structurally related subunits. EMBO J. *11*, 4767–4778.

Gao, Y., Thomas, J.O., Chow, R.L., Lee, G.-H., and Cowan, N.J. (1992). A cytoplasmic chaperonin that catalyzes β-actin folding. Cell *69*, 1043–1050.

Georgopoulos, C.P., Hendrix, R.W., Casjens, S.R., and Kaiser, A.D. (1973). Host participation in bacteriophage lambda head assembly. J. Mol. Biol. *76*, 45–60.

Gray, T.E., and Fersht, A.R. (1991). Cooperativity in ATP hydrolysis by GroEL is increased by GroES. FEBS Lett. *292*, 254–258.

Guagliardi, A., Cerchia, L., Bartolucci, S., and Rossi, M. (1994). The chaperonin from the archaeon Sulfolobus solfataricus promotes correct refolding and prevents thermal denaturation in vitro. Protein Sci. *3*, 1436–1443.

Hartl, F.-U. (1996). Molecular chaperones in cellular protein folding. Nature *381*, 571–580.

Hayer-Hartl, M.K., Martin, J., and Hartl, F.-U. (1995). Asymmetrical interaction of GroEL and GroES in the ATPase cycle of assisted protein folding. Science *269*, 836–841.

Hayer-Hartl, M.K., Weber, F., and Hartl, F.-U. (1996). Mechanism of chaperonin action: GroES binding and release can drive GroEL-mediated protein folding in the absence of ATP hydrolysis. EMBO J. *15*, 6111–6121.

Hemmingsen, S.M., Woolford, C., van der Vies, S.M., Tilly, K., Dennis, D.T., Georgopoulos, C.P., Hendrix, R.W., and Ellis, R.J. (1988). Homologous plant and bacterial proteins chaperone oligomeric protein assembly. Nature *333*, 330–334.

Horwich, A.L., Low, K.B., Fenton, W.A., Hirshfield, I.N., and Furtak, K. (1993). Folding in vivo of bacterial cytoplasmic proteins: role of GroEL. Cell *74*, 909–917.

Hunt, J.F., Weaver, A.J., Landry, S.J., Gierasch, L., and Deisenhofer, J. (1996). The crystal structure of the GroES co-chaperonin at 2.8 Å resolution. Nature *379*, 37–45.

Jones, T.A. (1978). A graphics model building and refinement system for macromolecules. J. Appl. Crystallogr. *11*, 268–272.

Kabsch, W., and Sander, C. (1983). Dictionary of protein secondary

structure: pattern recognition of hydrogen-bonded and geometrical features. Biopolymers *22*, 2577–2637.

Kabsch, W., Mannherz, H.G., Suck, D., Pai, E.F., and Holmes, K.C. (1990). Atomic structure of the actin DNase I complex. Nature *347*, 37–44.

Kim, S., Willison, K.R., and Horwich, A.L. (1994). Cytosolic chaperonin subunits have a conserved ATPase domain but diverged polypeptide-binding domains. TIBS *19*, 543–548.

Kleywegt, G.J., and Jones, T.A. (1994). Detection, delineation, measurement and display of cavities in macromolecular structures. Acta Crystallogr. *D50*, 178–185.

Klumpp, M., Baumeister, W., and Essen, L.-O. (1997). Structure of the substrate binding domain of the thermosome, an archaeal group II chaperonin. Cell *91*, 263–270.

Knapp, S., Schmidt-Krey, I., Hebert, H., Bergman, T., Jörnvall, H., and Ladenstein, R. (1994). The molecular chaperonin TF55 from the thermophilic archaeon Sulfolobus solfataricus. J. Mol. Biol. *242*, 397–407.

Kraulis, P. (1991). MOLSCRIPT: a program to produce both detailed and schematic plots of proteins. J. Appl. Crystallogr. *24*, 946–950.

Kubota, H., Hynes, G., Carne, A., Ashworth, A., and Willison, K. (1994). Identification of six Tcp-1-related genes encoding divergent subunits of the TCP-1-containing chaperonin. Curr. Biol. *4*, 89–99.

Langer, T., Pfeifer, G., Martin, J., Baumeister, W., and Hartl, F.-U. (1992). Chaperonin-mediated protein folding: GroES binds to one end of the GroEL cylinder, which accomodates the protein substrate within its central cavity. EMBO J. *11*, 4757–4765.

Laskowski, R.A., MacArthur, M.W., Moss, D.S., and Thornton, J.M. (1993). PROCHECK: a program to check the stereochemical quality of protein structures. J. Appl. Crystallogr. *26*, 283–291.

Leslie, A.G.W. (1991). Recent changes to the MOSFLM package for processing film and image plate data (Daresbury, Warrington WA44AD, UK: SERC Laboratory).

Lewis, V.A., Hynes, G.M., Zheng, D., Saibil, H., and Willison, K. (1992). T-complex polypeptide-1 is a subunit of a heteromeric particle in the eukaryotic cytosol. Nature *358*, 249–252.

Llorca, O., Marco, S., Carrascosa, J.L., and Valpuesta, J.M. (1994). The formation of symmetrical GroEL-GroES complexes in the presence of ATP. FEBS Lett. *345*, 181–186.

Mande, S.C., Mehra, V., Bloom, B.R., and Hol, W.G. J. (1996). Structure of the heat shock protein chaperonin-10 of Mycobacterium leprae. Science *271*, 203–207.

Marco, S., Carroscosa, J.L., and Valpuesta, J.M. (1994a). Reversible interaction of β-actin along the channel of the TCP-1 cytoplasmic chaperonin. Biophys. J. *67*, 364–368.

Marco, S., Ureña, D., Carrascosa, J.L., Waldmann, T., Peters, J., Hegerl, R., Pfeifer, G., Sack-Kongehl, H., and Baumeister, W. (1994b). The molecular chaperone TF55. Assessment of symmetry. FEBS Lett. *341*, 152–155.

Mayhew, M., da Silva, A.C.R., Martin, J., Erdjument-Bromage, H., Tempst, P., and Hartl, F.-U. (1996). Protein folding in the central cavity of the GroEL-GroES chaperonin complex. Nature *379*, 420–426.

Melki, R., and Cowan, N.J. (1994). Facilitated folding of actins and tubulins occurs via a nucleotide-dependent interaction between cytoplasmic chaperonin and distinctive folding intermediates. Mol. Cell. Biol. *14*, 2895–2904.

Melki, R., Batelier, G., Soulié, S., and Williams, R.C. (1997). Cytoplasmic chaperonin containing TCP-1: structural and functional characterization. Biochemistry *36*, 5817–5826.

Merrit, E.A., and Murphy, M.E.P. (1994). Raster3D Version 2.0. A program for photorealistic molecular graphics. Acta Crystallogr. *D50*, 869–873.

Nicholls, A., Bharadwaj, R., and Honig, B. (1993). GRASP—graphical representation and analysis of surface properties. Biophys. J. *64*, A166.

Nitsch, M., Klumpp, M., Lupas, A., and Baumeister, W. (1997). The thermosome: alternating α and β-subunits within the chaperonin of the archaeon Thermoplasma acidophilum. J. Mol. Biol. *267*, 142–149.

Phipps, B.M., Hoffmann, A., Stetter, K.O., and Baumeister, W. (1991). A novel ATPase complex selectively accumulated upon heat shock is a major cellular component of thermophilic archaebacteria. EMBO J. *10*, 1711–1722.

Phipps, B.M., Typke, D., Hegerl, R., Volker, S., Hoffmann, A., Stetter, K.O., and Baumeister, W. (1993). Structure of a molecular chaperone from a thermophilic archaebacterium. Nature *361*, 475–477.

Roseman, A.M., Chen, S., White, H., Braig, K., and Saibil, H.R. (1996). The chaperonin ATPase cycle: mechanism of allosteric switching and movements of substrate-binding domains in GroEL. Cell *87*, 241–251.

Rye, H.S., Burston, S.G., Fenton, W.A., Beechem, J.M., Xu, Z., Sigler, P.B., and Horwich, A.L. (1997). Distinct actions of cis and trans ATP within the double ring of the chaperonin GroEL. Nature *388*, 792–798.

Saibil, H.R., Zheng, D., Roseman, A.M., Hunter, A.S., Watson, G.M.F., Chen, S., auf der Mauer, A., O'Hara, B.P., Wood, S.P., Mann, N.H., et al. (1993). ATP induces large quaternary rearrangements in a cage-like chaperonin structure. Curr. Biol. *3*, 265–273.

Schägger, H., and von Jagow, G. (1987). Tricine-sodium dodecyl sulfate-polyacrylamide gel electrophoresis for the separation of proteins in the range from 1 to 100 kDa. Anal. Biochem. *166*, 368–379.

Schmidt, M., Rutkat, K., Rachel, R., Pfeifer, G., Jaenicke, R., Viitanen, P., Lorimer, G., and Buchner, J. (1994). Symmetric complexes of GroE chaperonins as part of the functional cycle. Science *265*, 656–659.

Sheldrick, G.M., Dauter, Z., Wilson, K.S., Hope, H., and Sieker, L.C. (1993). The application of direct methods of patterson interpretation to high-resolution native protein data. Acta Crystallogr. *D49*, 18–23.

Sondek, J., Lambright, D.G., Noel, J.P., Hamm, H.E., and Sigler, P.B. (1994). GTPase mechanism of G proteins from the 1.7-Å crystal structure of transducin αGDP $AlF_4^-$. Nature *372*, 276–279.

Staniforth, R., Burston, S.G., Atkinson, T., and Clarke, A.R. (1994). Affinity of chaperonin 60 for a protein substrate and its modulation by nucleotides and chaperonin 10. Biochem. J. *300*, 651–658.

Sternlicht, H., Farr, G.W., Sternlicht, M.L., Driscoll, J.K., Willison, K., and Yaffe, M.B. (1993). The t-complex polypeptide 1 complex is a chaperonin for tubulin and actin in vivo. Proc. Natl. Acad. Sci. USA *90*, 9422–9426.

Tilly, K., Murialdo, H., and Georgopoulos, C. (1981). Identification of a second Escherichia coli groE gene whose product is necessary for bacteriophage morphogenesis. Proc. Natl. Acad. Sci. USA *78*, 1629–1633.

Trent, J.D., Nimmesgern, E., Wall, J.S., Hartl, F.-U., and Howich, A.L. (1991). A molecular chaperone from a thermophilic archaebacterium is related to the eukaryotic protein t-complex polypeptide-1. Nature *354*, 490–493.

Turk, D. (1992). Weiterentwicklung eines Programms für Molekülgraphik und Elektrondichte-Manipulation und seine Anwendung auf verschiedene Protein-Strukturaufklärungen (München: Technische Universität) [Dissertation].

Viitanen, P.V., Gatenby, A.A., and Lorimer, G.H. (1992). Purified chaperonin 60 (GroEL) interacts with the nonnative states of a multitude of Escherichia coli proteins. Protein Sci. *1*, 363–369.

Waldmann, T., Nimmesgern, E., Nitsch, M., Peters, J., Pfeifer, G., Müller, S., Kellermann, J., Engel, A., Hartl, F.-U., and Baumeister, W. (1995). The thermosome of Thermoplasma acidophilum and its relationship to the eukaryotic chaperonin TRiC. Eur. J. Biochem. *227*, 848–856.

Weissman, J.S., Kashi, Y., Fenton, W.A., and Horwich, A.L. (1994). GroEL-mediated protein folding proceeds by multiple rounds of binding and release of nonnative forms. Cell *78*, 693–702.

Weissman, J.S., Hohl, C.M., Kovalenko, O., Kashi, Y., Chen, S., Braig, K., Saibil, H.R., Fenton, W.A., and Horwich, A.L. (1995). Mechanism of GroEL action: productive release of polypeptide from a sequestered position under GroES. Cell *83*, 577–587.

Weissman, J.S., Rye, H.S., Fenton, W.A., Beechem, J.M., and Horwich, A.L. (1996). Characterization of the active intermediate of a GroEL-GroES-mediated protein folding reaction. Cell *84*, 481–490.

Willison, K.R., and Kubota, H. (1994). The structure, function and genetics of the chaperonin containing TCP-1 (CCT) in eukaryotic

cytosol. In The Biology of Heat Shock Proteins and Molecular Chaperones, R.I. Morimoto, A. Tissieres, and C. Georgopoulos, eds. (Cold Spring Harbor, NY: Cold Spring Harbor Laboratory Press), pp. 299–312.

Xu, Z., Howich, A.L., and Sigler, P.B. (1997a). The crystal structure of the asymmetric GroEL-GroES-(ADP)7 chaperonin complex. Nature *388*, 741–750.

Xu, Y.-W., Moréra, S., Janin, J., and Cherfils, J. (1997b). $AlF_3$ mimics the transition state of protein phosphorylation in the crystal structure of nucleoside diphosphate kinase and MgADP. Proc. Natl. Acad. Sci. USA *94*, 3579–3583.

Yaffe, M.B., Farr, G.W., Miklos, D., Horwich, A.L., Sternlicht, M.L., and Sternlicht, H. (1992). TCP1 complex is a molecular chaperone in tubulin biogenesis. Nature *358*, 245–248.

Yifrach, O., and Horovitz, A. (1994). Two lines of allosteric communication in the oligomeric chaperonin GroEL are revealed by the single mutation Arg196→Ala. J. Mol. Biol. *243*, 397–401.

**Brookhaven Protein Data Bank ID Numbers**

Coordinates have been deposited with the Brookhaven Protein Data Bank (accession numbers 1A6D and 1A6E).